Heavy Higgs signal-background interference in $gg \rightarrow VV$ in the Standard Model plus real singlet

Nikolas Kauer and Claire O'Brien

Department of Physics, Royal Holloway, University of London, Egham Hill, Egham TW20 0EX, U.K.

E-mail: n.kauer@rhul.ac.uk, claire.obrien.2012@live.rhul.ac.uk

ABSTRACT: For the Standard Model extended with a real scalar singlet field, the modification of the heavy Higgs signal due to interference with the continuum background and the off-shell light Higgs contribution is studied for $gg \rightarrow ZZ, WW \rightarrow 4$ lepton processes at the Large Hadron Collider. Interference effects can range from $\mathcal{O}(10\%)$ to $\mathcal{O}(1)$ effects for integrated cross sections. Despite a strong cancellation between the heavy Higgs-continuum and the heavy Higgs-light Higgs interference, the full interference is clearly non-negligible and modifies the heavy Higgs line shape. A $|M_{VV} - M_{h2}| < \Gamma_{h2}$ cut mitigates interference effects to $\mathcal{O}(10\%)$ or less. A public program that allows to simulate the full interference is presented.

Contents

1 Introduction

In 2012, the ATLAS and CMS experiments at the CERN Large Hadron Collider (LHC) announced the discovery of a new scalar resonance with a mass of approximately 125 GeV [1]. The discovered particle is so far consistent with the Higgs boson predicted by the Standard Model (SM) Higgs mechanism [2], but many extensions to the SM preserve the minimal assumptions of an $SU(2)$ doublet which acquires a vacuum expectation value thus inducing a physical Higgs boson that couples to fermions and vector bosons in proportion to their mass, while also allowing for an expanded Higgs sector with additional, heavier (or lighter) Higgs-like scalar particles. The search for high-mass Higgs-like particles in the $gg \to H \to ZZ$ and $gg \to H \to WW$ channels at the LHC is ongoing [3–12].

  With inclusive NNLO signal uncertainties of $\mathcal{O}(10\%)$ in gluon-fusion Higgs production at the LHC, which can be further reduced by experimental selection cuts, it is important to study signal-background interference in the $H \to VV$ decay modes ($V = Z, W$), because it can be of similar size or larger for Higgs invariant masses above the weak-boson pair threshold. For Higgs invariant masses much larger than $2M_V$, the occurring sizeable Higgs-continuum interference is linked to the preservation of unitarity. In the SM, interference between the Higgs signal and continuum background in $gg\, (\to H) \to VV$ and including fully leptonic decays has been studied in refs. [13–27].[1] Higgs-continuum interference results for a heavy SM Higgs boson with a Γ_H/M_H ratio of $\mathcal{O}(10\%)$ or more have been presented in refs. [16–18, 20, 21, 23, 25]. We note that all Higgs-continuum interference calculations are at leading order (LO), except for refs. [20, 23, 27], where approximate higher-order corrections have been calculated.

  Since a Higgs boson with $M_H \approx 125$ GeV has been discovered, a theoretically consistent search for an additional Higgs boson has to be based on a model that is beyond the SM.

---

[1]We note that the interfering $gg \to VV$ continuum background at LO is formally part of the NNLO corrections to $pp \to VV$ [28, 29]. SM Higgs-continuum interference in the $H \to VV$ decay modes at a e^+e^- collider has been studied in ref. [30]. Predictions for $gg \to \ell\ell\nu\nu + 0, 1$ jets have been presented in ref. [31].

The simplest extension of the Higgs sector of the SM introduces an additional real scalar singlet field which is neutral under the SM gauge groups. The remaining viable parameter space of this 1-Higgs-Singlet extension of the SM (abbreviated by 1HSM) after LHC Run 1 has been studied in refs. [32, 33].[2] Here, we focus on the case where the additional Higgs boson is heavier than the discovered Higgs boson. In this case, the heavy Higgs signal is affected not only by sizeable interference with the continuum background, but also by a non-negligible interference with the off-shell tail of the light Higgs boson [19]. A calculation including full interference effects in a Higgs portal model has been carried out in ref. [37]. But, the occurring interference effects (which are discernible in the distributions shown in figure 8 of ref. [37]) have not been analysed quantitatively there.[3] A dedicated study of heavy Higgs-light Higgs interference in the 1HSM with an additional Z_2 symmetry was presented in ref. [38].[4]

In this paper, we extend the analysis of ref. [38] by taking into account the full signal-background interference which includes the heavy Higgs-continuum interference.[5] Furthermore, in addition to $gg \to h_2 \to ZZ \to 4$ leptons, where h_2 is the heavy Higgs boson, we also calculate results for $gg \to h_2 \to WW \to 4$ leptons. Our calculations are carried out with a new version of the parton-level integrator and event generator gg2VV, which we have made publicly available [41]. In section 2 we discuss the 1HSM and specify the used benchmark points. Calculational details are discussed in section 3. Integrated cross sections and differential distributions in M_{VV} for the heavy Higgs signal and its interference with the continuum background and off-shell light Higgs contribution are presented in section 4 for $gg \to h_2 \to ZZ \to \ell\bar{\ell}\ell'\bar{\ell}'$ and $gg \to h_2 \to W^-W^+ \to \ell\bar{\nu}\bar{\ell}'\nu'$. Conclusions are given in section 5.

2   Model

As minimal theoretically consistent model with two physical Higgs bosons, we consider the SM with an added real singlet field which is neutral under all SM gauge groups. The 1-Higgs-Singlet Extension of the SM has been extensively explored in the literature [42–62]. Higgs singlet models with an additional Z_2 symmetry have generated some interest recently because of the possibility of the additional Higgs boson being a dark matter candidate, but here we consider the most general extension. In the following, we give a brief summary of the model. A more detailed description can be found in refs. [62, 63].

The SM Higgs sector is extended by the addition of a new real scalar field, which is a singlet under all the gauge groups of the SM and which also gets a vacuum expectation value (VEV) under electroweak symmetry breaking. The most general gauge-invariant

---

[2]See also refs. [34–36].

[3]We note that we presented preliminary results which demonstrate the importance of heavy-light and heavy-continuum interference in September 2014 at the HP2 Workshop, Florence.

[4]For Higgs production in vector boson fusion, heavy-light interference in a two-Higgs model was studied in ref. [30] for an e^+e^- collider and in more detail including heavy-continuum interference in ref. [39] for the LHC.

[5]A similar study which numerically agrees with ours has subsequently appeared on the arXiv [40].

potential can be written as [43, 45]

$$V = \lambda \left(\Phi^\dagger \Phi - \frac{v^2}{2} \right)^2 + \frac{1}{2} M^2 s^2 + \lambda_1 s^4 + \lambda_2 s^2 \left(\Phi^\dagger \Phi - \frac{v^2}{2} \right) + \mu_1 s^3 + \mu_2 s \left(\Phi^\dagger \Phi - \frac{v^2}{2} \right), \quad (2.1)$$

where s is the real singlet scalar which is allowed to mix with the SM $SU(2)$ Higgs doublet, which in the unitary gauge can be written as

$$\Phi = \begin{pmatrix} 0 \\ (\phi + v)/\sqrt{2} \end{pmatrix} \quad (2.2)$$

with VEV $v \simeq 246$ GeV. Here it has already been exploited that (without the Z_2 symmetry) shifting the singlet field simply corresponds to a redefinition of the parameter coefficients and due to this freedom one can take the VEV of the singlet field to zero, which implies $M^2 > 0$. To avoid vacuum instability the quartic couplings must satisfy

$$\lambda > 0, \quad \lambda_1 > 0, \quad \lambda_2 > -2\sqrt{\lambda \lambda_1} \,. \quad (2.3)$$

The trilinear couplings μ_1 and μ_2 can have positive or negative sign. Substituting eq. (2.2) into eq. (2.1), one obtains the potential

$$V = \frac{\lambda}{4} \phi^4 + \lambda v^2 \phi^2 + \lambda v \phi^3 + \frac{1}{2} M^2 s^2 + \lambda_1 s^4 + \frac{\lambda_2}{2} \phi^2 s^2 + \lambda_2 v \phi s^2 + \mu_1 s^3 + \frac{\mu_2}{2} \phi^2 s + \mu_2 v \phi s \,. \quad (2.4)$$

The mass eigenstates can be parametrised in terms of a mixing angle θ as

$$h_1 = \phi \cos\theta - s \sin\theta \,, \quad (2.5)$$
$$h_2 = \phi \sin\theta + s \cos\theta \,, \quad (2.6)$$

where h_1 is assumed to be the lighter Higgs boson with a mass of approximately 125 GeV, and

$$\tan 2\theta = \frac{-\mu_2 v}{\lambda v^2 - \frac{1}{2} M^2} \quad (2.7)$$

with

$$-\frac{\pi}{4} < \theta < \frac{\pi}{4} \quad (2.8)$$

under the condition $M^2 > 2\lambda v^2$. The model has six independent parameters, which we choose to be $M_{h1}, M_{h2}, \theta, \mu_1, \lambda_1$ and λ_2. The dependent model parameters are:

$$\lambda = \frac{\cos(2\theta)\left(M_{h1}^2 - M_{h2}^2\right) + M_{h1}^2 + M_{h2}^2}{4v^2} \,, \quad (2.9)$$

$$M^2 = \frac{M_{h2}^2 - M_{h1}^2 + \sec(2\theta)\left(M_{h1}^2 + M_{h2}^2\right)}{2\sec(2\theta)} \,, \quad (2.10)$$

$$\mu_2 = -\tan(2\theta)\,\frac{\lambda v^2 - \frac{1}{2} M^2}{v} \,. \quad (2.11)$$

We set M_{h1} to 125 GeV in accordance with the mass of the observed resonance and study three values for the mass of the heavy Higgs resonance: $M_{h2} = 300$ GeV, $M_{h2} = 600$
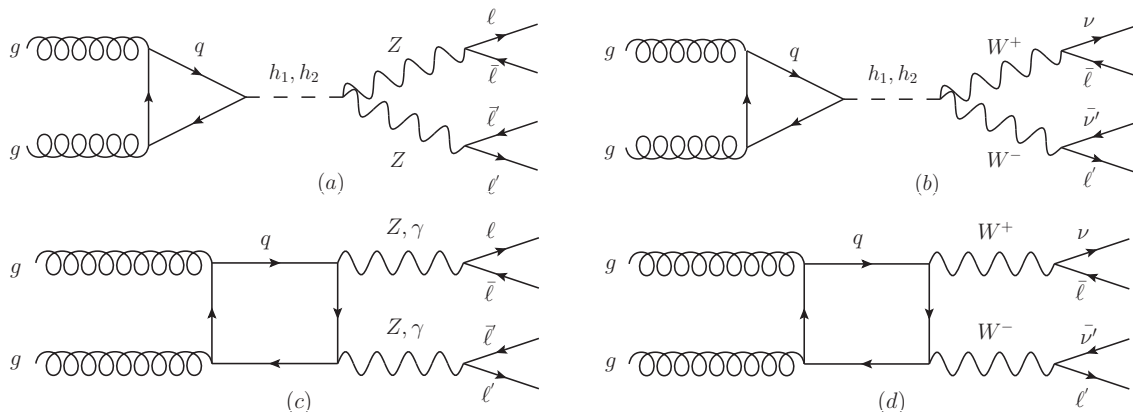
Figure 1. Representative Feynman graphs for $gg \ (\to \{h_1, h_2\}) \to ZZ, WW \to 4$ leptons. The heavy Higgs (h_2) graphs define the signal process, which interferes with the light Higgs (h_1) graphs (a,b). They also interfere with the gluon-induced continuum background graphs (c,d).

GeV and $M_{h2} = 900$ GeV. We choose the mixing angle θ so as not to alter the predicted light Higgs cross section too much. To illustrate how interference effects change with the mixing angle, we study the two values $\theta = \pi/15$ and $\theta = \pi/8$, which is consistent with current limits on the Higgs signal strength and does not appear to be in conflict with limits given in ref. [33], but strictly speaking these apply to the model with the additional Z_2 symmetry and are not directly applicable here. Furthermore, we consider model benchmark points with vanishing coupling parameters μ_1, λ_1 and λ_2. ($\lambda_1 > 0$ is treated as approximately zero.) We emphasise that this does not imply that the $h_2 \to h_1 h_1$ decay width is zero. For instance, for the mixing angle $\theta = \pi/8$ and $M_{h2} = 300$ (600) [900] GeV the branching ratio $\Gamma(h_2 \to h_1 h_1)/\Gamma_{h2}$ is 28% (20%) [19%]. The $h_2 \to h_1 h_1$ decay mode is therefore not suppressed in our study. Furthermore, the implementation in gg2VV is not restricted to benchmark points with vanishing μ_1, λ_1 and λ_2. Nonzero values of μ_1, λ_1 and λ_2 affect the calculation of the signal-background interference only via a change of the heavy Higgs width. In combination with FeynRules, our implementation in gg2VV therefore allows to calculate full signal-background interference effects for arbitrary benchmark points of the general 1-Higgs-Singlet Extension of the SM. See section 3 for further details. Ref. [62] gives bounds on the λ_1 and μ_1 parameters for $M_{h2} \lesssim 500$ GeV and a similar θ, which are in agreement with our choice of zero for these parameters. Our choice for the coupling parameters is also in agreement with upper limits on the combination of these parameters from experimental searches [64, 65].

3 Calculational details

In section 4 we present results calculated with a new version of gg2VV [17, 19, 21], which is publicly available [41]. Representative Feynman graphs for the light and heavy Higgs and interfering continuum background processes are shown in figure 1. The heavy Higgs (h_2) graphs define the signal process. They interfere with the light Higgs (h_1) graphs

		h_1	h_2		
	M [GeV]	125	300	600	900
$\theta = \pi/15$	Γ [GeV]	4.77358×10^{-3}	0.5383	6.42445	21.4215
$\theta = \pi/8$	Γ [GeV]	4.2577×10^{-3}	1.70204	20.7236	69.1805

Table 1. Widths of the physical Higgs bosons h_1 and h_2 in the 1-Higgs-Singlet Extension of the SM with mixing angles $\theta = \pi/15$ and $\theta = \pi/8$ as well as $\mu_1 = \lambda_1 = \lambda_2 = 0$.

and with the gluon-induced continuum background graphs. The amplitudes are calculated using a modified (for compatibility only) output of FeynArts/FormCalc [66, 67], using a custom coded UFO [68] model file generated by FeynRules [69]. The Higgs boson widths are calculated using FeynRules for consistency. The used width values are given in table 1. The PDF set MSTW2008LO [70] with default α_s is used and the CKM matrix is approximated by the unit matrix, which causes a negligible error [17]. As input parameters, we use the specification of the LHC Higgs Cross Section Working Group in App. A of ref. [71] with G_μ scheme and LO weak boson widths for consistency. More specifically, $M_W = 80.398$ GeV, $M_Z = 91.1876$ GeV, $\Gamma_W = 2.141$ GeV, $\Gamma_Z = 2.4952$ GeV, $M_t = 172.5$ GeV, $M_b = 4.75$ GeV, $G_F = 1.16637 \cdot 10^{-5}$ GeV^{-2} are used. Finite top and bottom quark mass effects are included. Lepton masses are neglected. A fixed-width Breit-Wigner propagator is employed for the weak bosons and the Higgs boson. The width parameter of the complex pole of the Higgs propagator is defined in eq. (16) of ref. [72]. The box graphs shown in figure 1(c,d) are affected by numerical instabilities when Gram determinants approach zero. In these critical phase space regions the amplitude is evaluated in quadruple precision. Residual instabilities are eliminated by requiring that $p_{T,W}$ and $p_{T,Z}$ are larger than 1 GeV. This criterion is also applied to the Higgs amplitudes, which are not affected by numerical instabilities, to obtain consistent cross section-level results. The numerical effect of this technical cut has been shown to be small [17, 22]. Furthermore, minimal selection cuts are applied: $M_{\ell\bar{\ell}} > 4$ GeV and $M_{\ell'\bar{\ell}'} > 4$ GeV cuts are applied for the $gg \to Z(\gamma^*)Z(\gamma^*) \to \ell\bar{\ell}\ell'\bar{\ell}'$ process to eliminate the soft photon singularities. The renormalisation and factorisation scales are set to $M_{VV}/2$ and the pp collision energy is $\sqrt{s} = 8$ TeV.

The phase space integration is carried out using the multi-channel Monte Carlo integration technique [73], in which every kinematic structure has its own mapping from random variables to the phase space configuration such that singularities or peaks in the amplitude are compensated, and the inverse Jacobi determinants of all mappings are summed to give the inverse weight at each phase space point. This approach has the advantage of a straightforward systematic extension from the SM to two-Higgs models: an extra channel with a mapping for the heavy Higgs resonance is added. The multi-channel technique has been implemented in the new version of gg2VV, and has been tested thoroughly. Each mapping was phase space integrated individually to check that the result matches the analytically known phase space volume for massless final state particles. Cross sections for the continuum background and h_1 only contributions[6] to the processes considered here were

---

[6] without mixing, i.e. $\theta = 0$

found to be in agreement with the results of ref. [21], which were calculated using a previous version of gg2VV with a different phase space implementation based on a decomposition into sections. Furthermore, results for similar processes calculated using the same code show excellent agreement with a fully independent implementation [74].

4 Results

In this section we present integrated and differential cross section-level results for the h_2 signal (S) and its interference (I) at the LHC for the processes

$$gg \ (\to \{h_1, h_2\}) \to Z(\gamma^*)Z(\gamma^*) \to \ell\bar{\ell}\ell'\bar{\ell}' \tag{4.1}$$

and

$$gg \ (\to \{h_1, h_2\}) \to W^-W^+ \to \ell\bar{\nu}\bar{\ell}'\nu' \tag{4.2}$$

with input parameters, settings and cuts as described in section 3. The following notation is used:

$$S \sim |\mathcal{M}_{h2}|^2 \tag{4.3}$$

$$I_{h1} \sim 2\,\mathrm{Re}(\mathcal{M}_{h2}^* \mathcal{M}_{h1}) \tag{4.4}$$

$$I_{bkg} \sim 2\,\mathrm{Re}(\mathcal{M}_{h2}^* \mathcal{M}_{bkg}) \tag{4.5}$$

$$I_{full} = I_{h1} + I_{bkg} \tag{4.6}$$

$$R_i = \frac{S + I_i}{S}\,. \tag{4.7}$$

The interference of the heavy Higgs signal with the light Higgs and continuum background is given separately. We also give the combined interference to illustrate the overall effect. The ratios R_{h1}, R_{bkg} and R_{full} illustrate the relative change of the heavy Higgs signal due to interference with the light Higgs and continuum background amplitude contributions. Integrated results for processes 4.1 and 4.2 are shown in tables 2–5. As illustrated by the differential distributions shown below, a $|M_{VV} - M_{h2}| < \Gamma_{h2}$ window cut is an effective means to eliminate or mitigate the interference.[7] Therefore, integrated results with window cut are presented in tables 6–9.

Corresponding M_{VV} distributions for processes 4.1 and 4.2 and $M_{h2} = 300, 600, 900$ GeV are shown in figures 2–15. Results for the heavy Higgs signal and including interference with the light Higgs and the continuum background are displayed. Where appropriate, vertical dashed lines at $M_{VV} = M_{h2} \pm \Gamma_{h2}$ are used to visualize the effect of a $|M_{VV} - M_{h2}| < \Gamma_{h2}$ window cut. For invariant VV masses with negative signal plus interference, the distributions are shown in figures 6 and 13.

As seen in the tables and figures, interference effects increase significantly with increasing heavy Higgs mass. They can range from $\mathcal{O}(10\%)$ to $\mathcal{O}(1)$ effects for integrated cross sections. With window cut we find that interference effects are mitigated to $\mathcal{O}(10\%)$ or

---

[7]For process 4.2, an invariant M_{WW} cut cannot be applied experimentally. However, a transverse mass cut is feasible.

$gg \to h_2 \to ZZ \to \ell\bar{\ell}\ell'\bar{\ell}'$ σ [fb], pp, $\sqrt{s} = 8$ TeV min. cuts, $\theta = \pi/15$		interference			ratio		
M_{h2} [GeV]	S	I_{h1}	I_{bkg}	I_{full}	R_{h1}	R_{bkg}	R_{full}
300	0.033453(7)	0.00392(2)	0.00105(2)	0.00499(2)	1.1171(6)	1.0315(7)	1.1492(6)
600	0.005223(4)	-0.001738(8)	0.001730(9)	-9(4)e-06	0.667(2)	1.331(2)	0.998(2)
900	0.0005088(4)	-0.001151(2)	0.001043(3)	-0.0001092(9)	-1.263(5)	3.049(5)	0.785(2)

Table 2. Cross sections for $gg \, (\to \{h_1, h_2\}) \to ZZ \to \ell\bar{\ell}\ell'\bar{\ell}'$ in pp collisions at $\sqrt{s} = 8$ TeV at loop-induced leading order in the 1-Higgs-Singlet Extension of the SM with $M_{h1} = 125$ GeV, $M_{h2} = 300, 600, 900$ GeV and mixing angle $\theta = \pi/15$. Results for the heavy Higgs (h_2) signal (S) and its interference with the light Higgs (I_{h1}) and the continuum background (I_{bkg}) and the full interference (I_{full}) are given. The ratio $R_i = (S + I_i)/S$ illustrates the relative change of the heavy Higgs signal due to interference with the light Higgs and continuum background amplitude contributions. Minimal cuts are applied (see main text). Cross sections are given for a single lepton flavour combination. The integration error is displayed in brackets.

$gg \to h_2 \to ZZ \to \ell\bar{\ell}\ell'\bar{\ell}'$ σ [fb], pp, $\sqrt{s} = 8$ TeV min. cuts, $\theta = \pi/8$		interference			ratio		
M_{h2} [GeV]	S	I_{h1}	I_{bkg}	I_{full}	R_{h1}	R_{bkg}	R_{full}
300	0.12209(9)	0.0119(1)	0.00358(5)	0.01545(4)	1.097(2)	1.029(2)	1.127(2)
600	0.01821(2)	-0.00498(2)	0.00568(2)	0.000694(8)	0.727(2)	1.312(2)	1.038(2)
900	0.001781(2)	-0.003277(5)	0.003396(5)	0.000118(3)	-0.840(3)	2.906(4)	1.066(2)

Table 3. Cross sections for $gg \, (\to \{h_1, h_2\}) \to ZZ \to \ell\bar{\ell}\ell'\bar{\ell}'$ in pp collisions in the 1-Higgs-Singlet Extension of the SM with mixing angle $\theta = \pi/8$. Other details as in table 2.

$gg \to h_2 \to W^-W^+ \to \ell\bar{\nu}\bar{\ell}'\nu'$ σ [fb], pp, $\sqrt{s} = 8$ TeV min. cuts, $\theta = \pi/15$		interference			ratio		
M_{h2} [GeV]	S	I_{h1}	I_{bkg}	I_{full}	R_{h1}	R_{bkg}	R_{full}
300	0.3752(3)	0.0391(9)	-0.0132(7)	0.0254(5)	1.104(3)	0.965(3)	1.068(2)
600	0.05380(4)	-0.0191(2)	0.0289(2)	0.00957(8)	0.645(3)	1.536(4)	1.178(2)
900	0.005149(4)	-0.01217(6)	0.01519(4)	0.00300(3)	-1.36(2)	3.950(9)	1.582(5)

Table 4. Cross sections for $gg \, (\to \{h_1, h_2\}) \to W^-W^+ \to \ell\bar{\nu}\bar{\ell}'\nu'$ in pp collisions at $\sqrt{s} = 8$ TeV in the 1-Higgs-Singlet Extension of the SM with $M_{h1} = 125$ GeV, $M_{h2} = 300, 600, 900$ GeV and mixing angle $\theta = \pi/15$. Other details as in table 2.

less. We note that the heavy Higgs-continuum background interference is negative above M_{h2} and positive below M_{h2}, while the heavy Higgs-light Higgs interference has the opposite behaviour. Consequently, in the heavy Higgs resonance region a strong cancellation occurs when both interference contributions are added. It is therefore essential to take both contributions into account in phenomenological and experimental studies. Despite

$gg \to h_2 \to W^-W^+ \to \ell\bar{\nu}\ell'\nu'$ σ [fb], pp, $\sqrt{s} = 8$ TeV min. cuts, $\theta = \pi/8$		interference			ratio		
M_{h2} [GeV]	S	I_{h1}	I_{bkg}	I_{full}	R_{h1}	R_{bkg}	R_{full}
300	1.368(2)	0.118(2)	-0.045(2)	0.0712(9)	1.086(2)	0.967(2)	1.052(2)
600	0.1875(2)	-0.0548(3)	0.0940(4)	0.0389(3)	0.708(2)	1.501(3)	1.207(2)
900	0.01806(2)	-0.03467(8)	0.0495(2)	0.01478(7)	-0.920(5)	3.742(7)	1.818(5)

Table 5. Cross sections for $gg \ (\to \{h_1, h_2\}) \to W^-W^+ \to \ell\bar{\nu}\ell'\nu'$ in pp collisions in the 1-Higgs-Singlet Extension of the SM with mixing angle $\theta = \pi/8$. Other details as in table 4.

$gg \to h_2 \to ZZ \to \ell\bar{\ell}\ell'\bar{\ell}'$ σ [fb], pp, $\sqrt{s} = 8$ TeV min. cuts & $|M_{VV} - M_{h2}| < \Gamma_{h2}$ $\theta = \pi/15$		interference			ratio		
M_{h2} [GeV]	S	I_{h1}	I_{bkg}	I_{full}	R_{h1}	R_{bkg}	R_{full}
300	0.02352(2)	3.8(4)e-06	0.001583(3)	0.001586(3)	1.000(2)	1.067(2)	1.067(2)
600	0.003719(4)	-1.7(2)e-05	0.000288(2)	0.000271(2)	0.995(2)	1.077(2)	1.073(2)
900	0.0003606(3)	-1.35(2)e-05	8.56(3)e-05	7.21(4)e-05	0.963(2)	1.237(2)	1.200(2)

Table 6. Cross sections for $gg \ (\to \{h_1, h_2\}) \to ZZ \to \ell\bar{\ell}\ell'\bar{\ell}'$ in pp collisions at $\sqrt{s} = 8$ TeV in the 1-Higgs-Singlet Extension of the SM with $M_{h1} = 125$ GeV, $M_{h2} = 300, 600, 900$ GeV and mixing angle $\theta = \pi/15$. An additional window cut $|M_{ZZ} - M_{h2}| < \Gamma_{h2}$ is applied. Other details as in table 2.

$gg \to h_2 \to ZZ \to \ell\bar{\ell}\ell'\bar{\ell}'$ σ [fb], pp, $\sqrt{s} = 8$ TeV min. cuts & $|M_{VV} - M_{h2}| < \Gamma_{h2}$ $\theta = \pi/8$		interference			ratio		
M_{h2} [GeV]	S	I_{h1}	I_{bkg}	I_{full}	R_{h1}	R_{bkg}	R_{full}
300	0.08537(8)	3.6(4)e-05	0.005371(9)	0.00541(1)	1.000(2)	1.063(2)	1.063(2)
600	0.01323(2)	-0.000174(4)	0.001058(4)	0.000884(6)	0.987(2)	1.080(2)	1.067(2)
900	0.001283(1)	-0.0001316(9)	0.000373(1)	0.000241(2)	0.897(2)	1.290(2)	1.188(2)

Table 7. Cross sections for $gg \ (\to \{h_1, h_2\}) \to ZZ \to \ell\bar{\ell}\ell'\bar{\ell}'$ in pp collisions in the 1-Higgs-Singlet Extension of the SM with mixing angle $\theta = \pi/8$. Other details as in table 6.

the occurring cancellation, the full interference is clearly non-negligible and modifies the heavy Higgs line shape. We find overall $\mathcal{O}(10\%)$ effects for integrated cross sections, even if a window cut is applied. The results for $\theta = \pi/15$ and $\theta = \pi/8$ are in qualitative agreement. Relative interference effects show a mild quantitative dependence on the mixing angle.

We note that our results for heavy Higgs-light Higgs interference are qualitatively in agreement with those given in ref. [38], where this interference is considered for $gg \to \{h_1, h_2\} \to ZZ \to 4\ell$, but in the 1HSM model with an extra Z_2 symmetry.

$gg \to h_2 \to W^-W^+ \to \ell\bar{\nu}\bar{\ell}'\nu'$ σ [fb], pp, $\sqrt{s} = 8$ TeV min. cuts & $|M_{VV} - M_{h2}| < \Gamma_{h2}$		interference			ratio		
$\theta = \pi/15$							
M_{h2} [GeV]	S	I_{h1}	I_{bkg}	I_{full}	R_{h1}	R_{bkg}	R_{full}
300	0.3352(3)	3.8(6)e-05	0.00959(6)	0.00963(7)	1.000(2)	1.029(2)	1.029(2)
600	0.04859(5)	-0.000188(4)	0.00419(3)	0.00401(3)	0.996(2)	1.086(2)	1.082(2)
900	0.004635(5)	-0.000137(3)	0.000929(5)	0.000792(5)	0.970(2)	1.200(2)	1.171(2)

Table 8. Cross sections for $gg \ (\to \{h_1, h_2\}) \to W^-W^+ \to \ell\bar{\nu}\bar{\ell}'\nu'$ in pp collisions at $\sqrt{s} = 8$ TeV in the 1-Higgs-Singlet Extension of the SM with $M_{h1} = 125$ GeV, $M_{h2} = 300, 600, 900$ GeV and mixing angle $\theta = \pi/15$. An additional window cut $|M_{WW} - M_{h2}| < \Gamma_{h2}$ is applied. Other details as in table 2.

| $gg \to h_2 \to W^-W^+ \to \ell\bar{\nu}\bar{\ell}'\nu'$ σ [fb], pp, $\sqrt{s} = 8$ TeV min. cuts & $|M_{VV} - M_{h2}| < \Gamma_{h2}$		interference			ratio		
$\theta = \pi/8$							
M_{h2} [GeV]	S	I_{h1}	I_{bkg}	I_{full}	R_{h1}	R_{bkg}	R_{full}
300	0.9578(9)	0.00034(2)	0.0324(2)	0.0329(2)	1.000(2)	1.034(2)	1.034(2)
600	0.1361(2)	-0.00184(2)	0.01578(6)	0.01394(3)	0.987(2)	1.116(2)	1.102(2)
900	0.01298(1)	-0.001340(7)	0.00429(2)	0.002952(7)	0.897(2)	1.331(2)	1.227(2)

Table 9. Cross sections for $gg \ (\to \{h_1, h_2\}) \to W^-W^+ \to \ell\bar{\nu}\bar{\ell}'\nu'$ in pp collisions in the 1-Higgs-Singlet Extension of the SM with mixing angle $\theta = \pi/8$. Other details as in table 8.
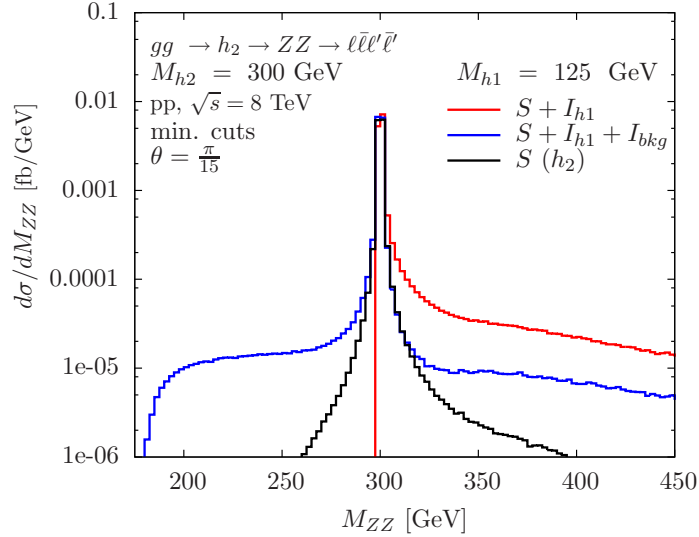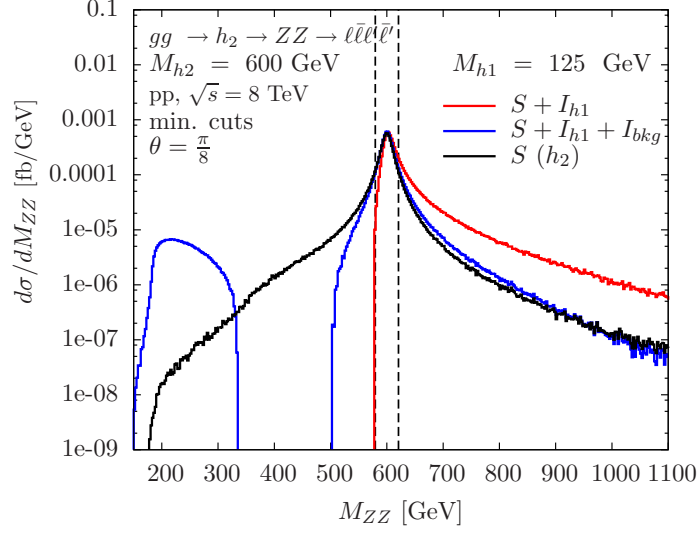

Figure 2. Invariant ZZ mass distributions for $gg \ (\to \{h_1, h_2\}) \to ZZ \to \ell\bar{\ell}\ell'\bar{\ell}'$ in pp collisions at $\sqrt{s} = 8$ TeV at loop-induced leading order in the 1-Higgs-Singlet Extension of the SM with $M_{h1} = 125$ GeV, $M_{h2} = 300$ GeV and mixing angle $\theta = \pi/15$. Results for the heavy Higgs (h_2) signal (S) and including interference with the light Higgs ($S + I_{h1}$) and the continuum background ($S + I_{h1} + I_{bkg}$) are shown. Minimal cuts are applied (see main text). Other details as in table 2.
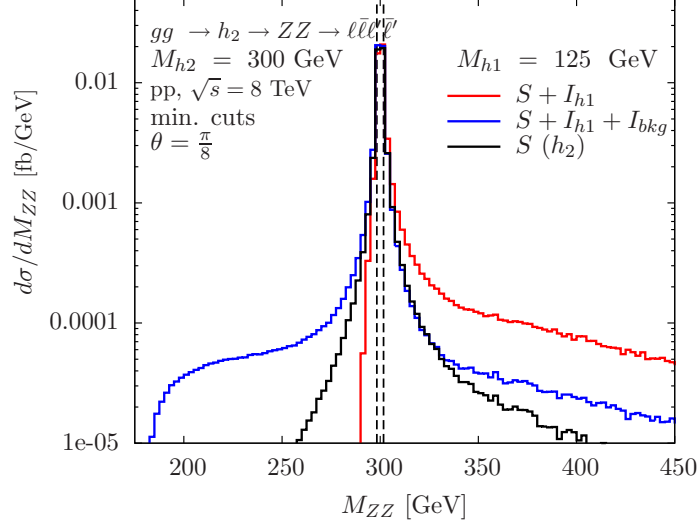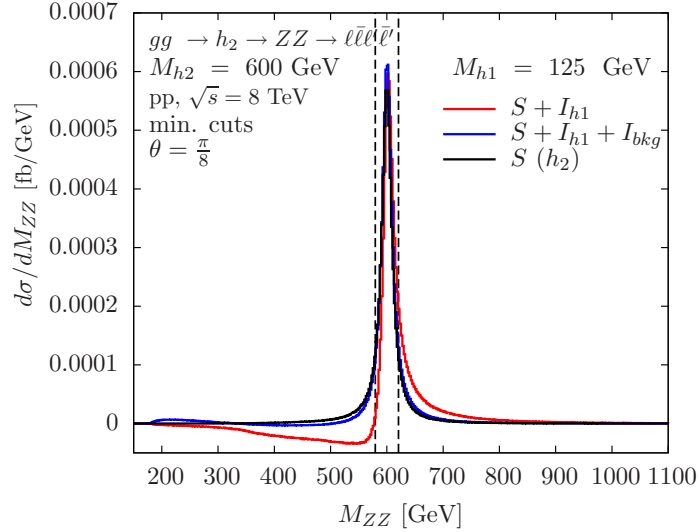
Figure 3. Invariant ZZ mass distributions for $gg \, (\to \{h_1, h_2\}) \to ZZ \to \ell\bar{\ell}\ell'\bar{\ell}'$ in pp collisions in the 1-Higgs-Singlet Extension of the SM with mixing angle $\theta = \pi/8$. Vertical dashed lines are shown at $M_{VV} = M_{h2} \pm \Gamma_{h2}$. Other details as in figure 2.
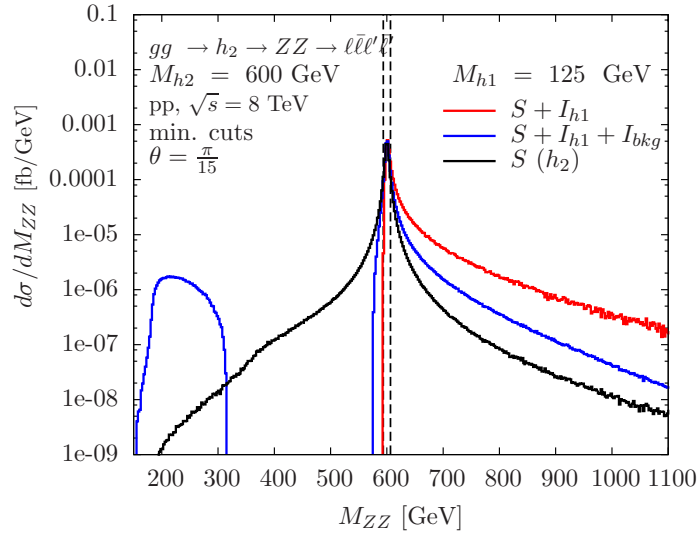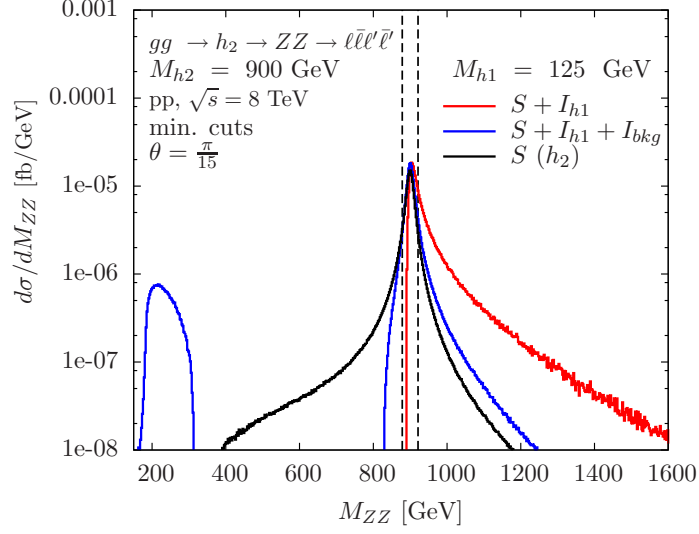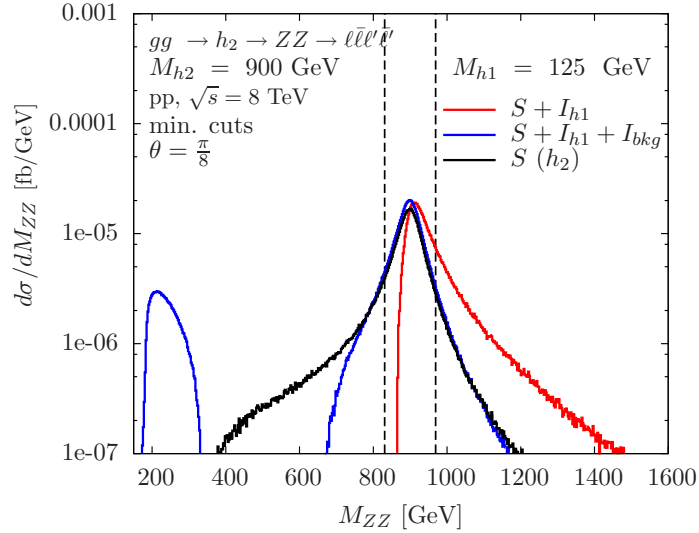

Figure 4. Invariant ZZ mass distributions for $gg \, (\to \{h_1, h_2\}) \to ZZ \to \ell\bar{\ell}\ell'\bar{\ell}'$ in pp collisions at $\sqrt{s} = 8$ TeV in the 1-Higgs-Singlet Extension of the SM with $M_{h1} = 125$ GeV, $M_{h2} = 600$ GeV and mixing angle $\theta = \pi/15$. Other details as in figure 2.

Figure 5. Invariant ZZ mass distributions for $gg \, (\to \{h_1, h_2\}) \to ZZ \to \ell\bar{\ell}\ell'\bar{\ell}'$ in pp collisions in the 1-Higgs-Singlet Extension of the SM with mixing angle $\theta = \pi/8$. Other details as in figure 4.
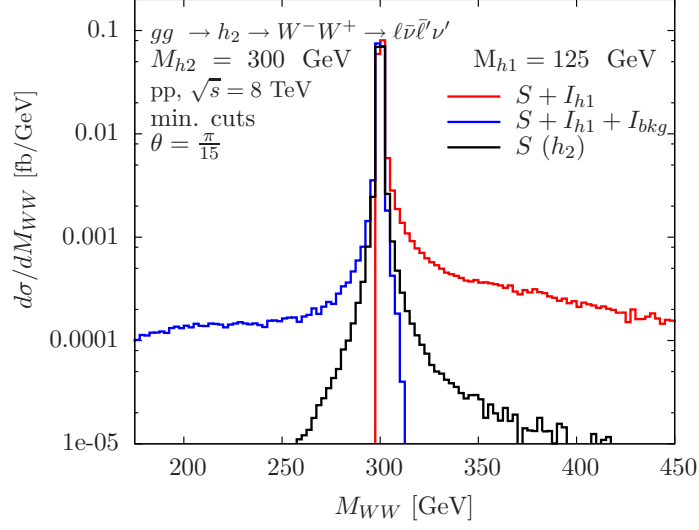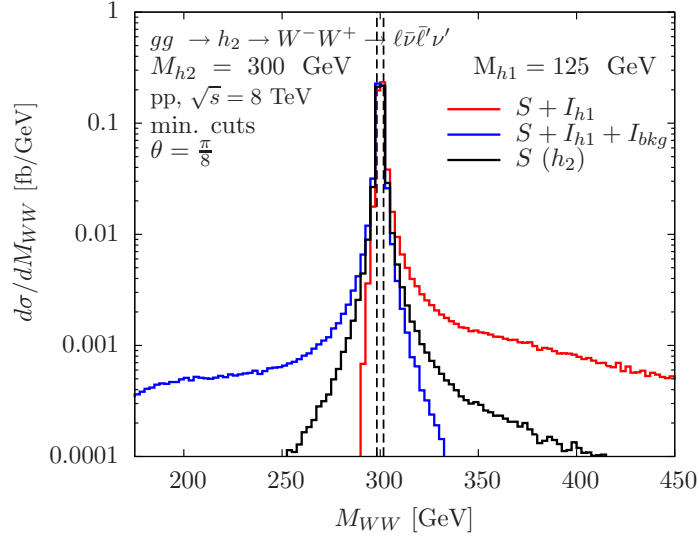

Figure 6. Invariant ZZ mass distributions for $gg \, (\to \{h_1, h_2\}) \to ZZ \to \ell\bar{\ell}\ell'\bar{\ell}'$ in pp collisions in the 1-Higgs-Singlet Extension of the SM with mixing angle $\theta = \pi/8$. As figure 5, but with linear $d\sigma/dM_{ZZ}$ scale, to illustrate negative $S + I_{h1}$ and $S + I_{h1} + I_{bkg}$.

Figure 7. Invariant ZZ mass distributions for $gg \, (\to \{h_1, h_2\}) \to ZZ \to \ell\bar{\ell}\ell'\bar{\ell}'$ in pp collisions at $\sqrt{s} = 8$ TeV in the 1-Higgs-Singlet Extension of the SM with $M_{h1} = 125$ GeV, $M_{h2} = 900$ GeV and mixing angle $\theta = \pi/15$. Other details as in figure 2.
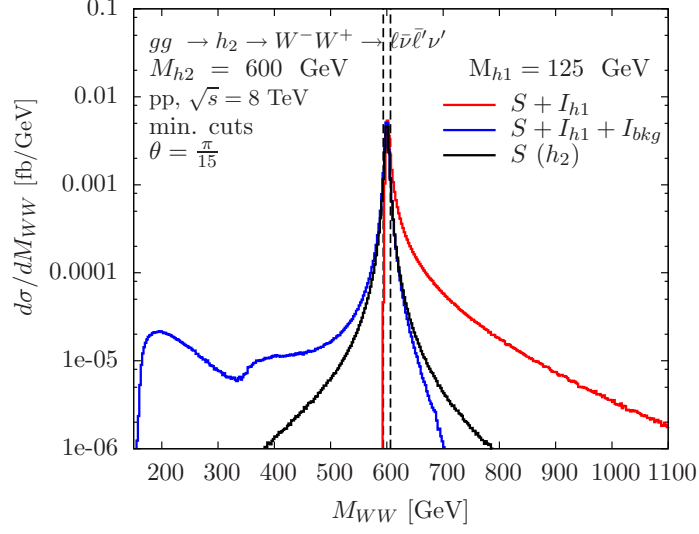

Figure 8. Invariant ZZ mass distributions for $gg \, (\to \{h_1, h_2\}) \to ZZ \to \ell\bar{\ell}\ell'\bar{\ell}'$ in pp collisions in the 1-Higgs-Singlet Extension of the SM with mixing angle $\theta = \pi/8$. Other details as in figure 7.
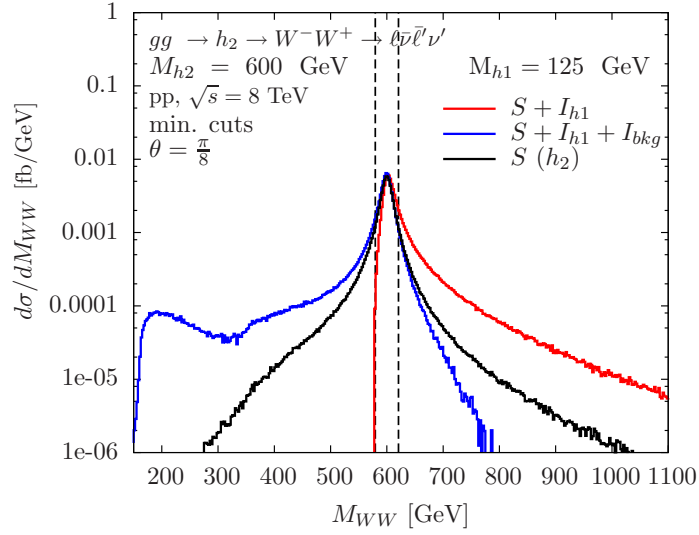
Figure 9. Invariant WW mass distributions for $gg \ (\to \{h_1, h_2\}) \to W^-W^+ \to \ell\bar{\nu}\bar{\ell}'\nu'$ in pp collisions at $\sqrt{s} = 8$ TeV in the 1-Higgs-Singlet Extension of the SM with $M_{h1} = 125$ GeV, $M_{h2} = 300$ GeV and mixing angle $\theta = \pi/15$. Other details as in figure 2.
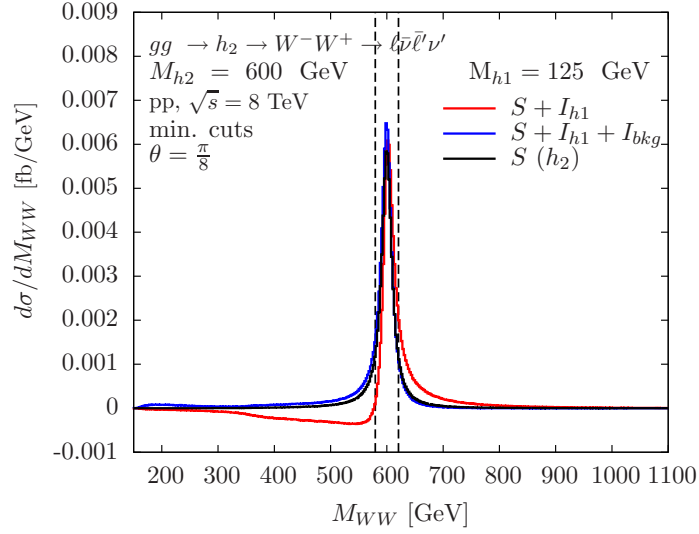

Figure 10. Invariant WW mass distributions for $gg \ (\to \{h_1, h_2\}) \to W^-W^+ \to \ell\bar{\nu}\bar{\ell}'\nu'$ in pp collisions in the 1-Higgs-Singlet Extension of the SM with mixing angle $\theta = \pi/8$. Other details as in figure 9.
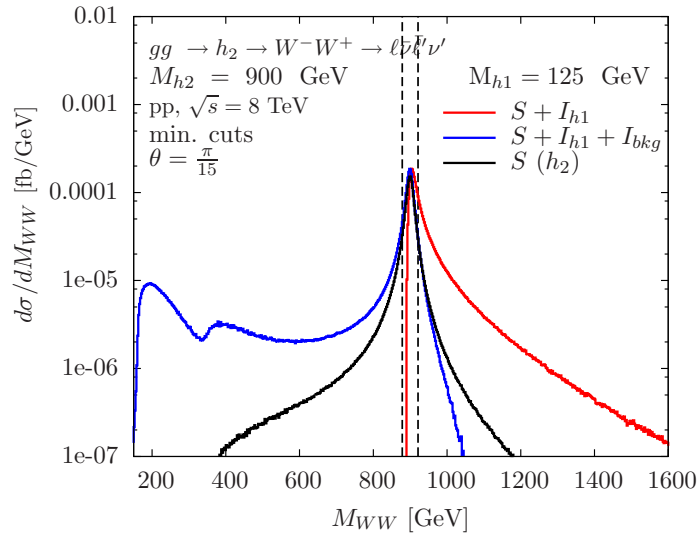
Figure 11. Invariant WW mass distributions for $gg \ (\to \{h_1, h_2\}) \to W^-W^+ \to \ell\bar{\nu}\bar{\ell}'\nu'$ in pp collisions at $\sqrt{s} = 8$ TeV in the 1-Higgs-Singlet Extension of the SM with $M_{h1} = 125$ GeV, $M_{h2} = 600$ GeV and mixing angle $\theta = \pi/15$. Other details as in figure 2.

Figure 12. Invariant WW mass distributions for $gg \ (\to \{h_1, h_2\}) \to W^-W^+ \to \ell\bar{\nu}\bar{\ell}'\nu'$ in pp collisions in the 1-Higgs-Singlet Extension of the SM with mixing angle $\theta = \pi/8$. Other details as in figure 11.
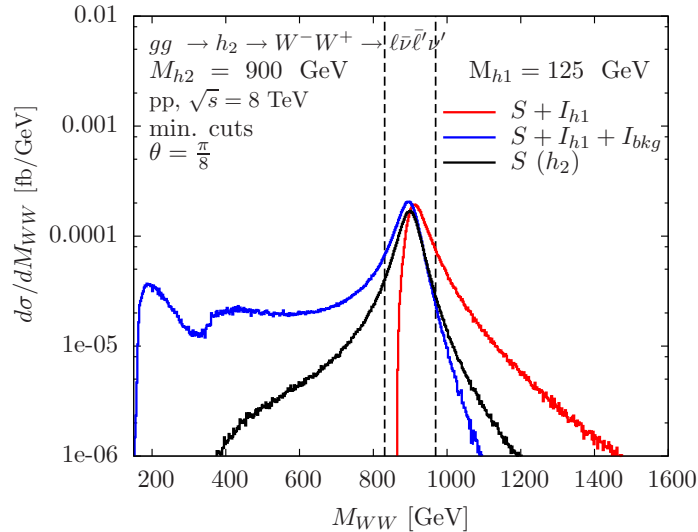
Figure 13. Invariant WW mass distributions for $gg \ (\to \{h_1, h_2\}) \to W^- W^+ \to \ell \bar{\nu} \bar{\ell}' \nu'$ in pp collisions in the 1-Higgs-Singlet Extension of the SM with mixing angle $\theta = \pi/8$. As figure 12, but with linear $d\sigma/dM_{WW}$ scale, to illustrate negative $S + I_{h1}$.

Figure 14. Invariant WW mass distributions for $gg \ (\to \{h_1, h_2\}) \to W^- W^+ \to \ell \bar{\nu} \bar{\ell}' \nu'$ in pp collisions at $\sqrt{s} = 8$ TeV in the 1-Higgs-Singlet Extension of the SM with $M_{h1} = 125$ GeV, $M_{h2} = 900$ GeV and mixing angle $\theta = \pi/15$. Other details as in figure 2.

Figure 15. Invariant WW mass distributions for $gg \, (\to \{h_1, h_2\}) \to W^- W^+ \to \ell \bar{\nu} \bar{\ell}' \nu'$ in pp collisions in the 1-Higgs-Singlet Extension of the SM with mixing angle $\theta = \pi/8$. Other details as in figure 14.

5   Conclusions

In the 1-Higgs-Singlet Extension of the SM, the modification of the heavy Higgs (h_2) signal due to interference with the continuum background and the off-shell light Higgs (h_1) contribution has been studied for the $gg \, (\to \{h_1, h_2\}) \to Z(\gamma^*)Z(\gamma^*) \to \ell \bar{\ell} \ell' \bar{\ell}'$ and $gg \, (\to \{h_1, h_2\}) \to W^- W^+ \to \ell \bar{\nu} \bar{\ell}' \nu'$ processes at the LHC. Interference effects increase significantly with increasing heavy Higgs mass. They can range from $\mathcal{O}(10\%)$ to $\mathcal{O}(1)$ effects for integrated cross sections. With a $|M_{VV} - M_{h2}| < \Gamma_{h2}$ window cut, we find that interference effects are mitigated to $\mathcal{O}(10\%)$ or less. We find that the heavy Higgs-continuum background interference is negative above M_{h2} and positive below M_{h2}, while the heavy Higgs-light Higgs interference has the opposite behaviour. Consequently, in the heavy Higgs resonance region a strong cancellation occurs when both interference contributions are added. It is therefore essential to take both contributions into account in phenomenological and experimental studies. Despite the occurring cancellation, the full interference is clearly non-negligible and modifies the heavy Higgs line shape. We find overall $\mathcal{O}(10\%)$ effects for integrated cross sections, even if a window cut is applied to mitigate the interference effects. Our calculations have been carried out with a parton-level integrator and event generator, which we have made publicly available.

Acknowledgments

References

[1] G. Aad *et al.* [ATLAS Collaboration], *Observation of a new particle in the search for the Standard Model Higgs boson with the ATLAS detector at the LHC*, Phys. Lett. B **716** (2012) 1 [arXiv:1207.7214 [hep-ex]]; S. Chatrchyan *et al.* [CMS Collaboration], *Observation of a new boson at a mass of 125 GeV with the CMS experiment at the LHC*, Phys. Lett. B **716** (2012) 30 [arXiv:1207.7235 [hep-ex]].

[2] P. W. Higgs, *Broken symmetries, massless particles and gauge fields*, Phys. Lett. **12** (1964) 132; P. W. Higgs, *Broken symmetries and the masses of gauge bosons*, Phys. Rev. Lett. **13** (1964) 508; P. W. Higgs, *Spontaneous symmetry breakdown without massless bosons*, Phys. Rev. **145** (1966) 1156; F. Englert and R. Brout, *Broken symmetry and the mass of gauge vector mesons*, Phys. Rev. Lett. **13** (1964) 321; G. S. Guralnik, C. R. Hagen and T. W. B. Kibble, *Global conservation laws and massless particles*, Phys. Rev. Lett. **13** (1964) 585.

[3] G. Aad *et al.* [ATLAS Collaboration], *Search for the Standard Model Higgs boson in the decay channel $H \to ZZ^{(*)} \to 4\ell$ with 4.8 fb^{-1} of pp collision data at $\sqrt{s} = 7$ TeV with ATLAS*, Phys. Lett. B **710** (2012) 383 [arXiv:1202.1415 [hep-ex]].

[4] S. Chatrchyan *et al.* [CMS Collaboration], *Search for the Standard Model Higgs boson in the decay channel $H \to ZZ \to 4$ leptons in pp collisions at $\sqrt{s} = 7$ TeV*, Phys. Rev. Lett. **108** (2012) 111804 [arXiv:1202.1997 [hep-ex]].

[5] S. Chatrchyan *et al.* [CMS Collaboration], *Search for a Higgs boson in the decay channel $H \to ZZ^{(*)} \to q\bar{q}\ell^-\ell^+$ in pp collisions at $\sqrt{s} = 7$ TeV*, JHEP **1204** (2012) 036 [arXiv:1202.1416 [hep-ex]].

[6] S. Chatrchyan *et al.* [CMS Collaboration], *Search for a Standard Model-like Higgs boson with a mass in the range 145 to 1000 GeV at the LHC*, Eur. Phys. J. C **73** (2013) 6, 2469 [arXiv:1304.0213 [hep-ex]].

[7] G. Aad *et al.* [ATLAS Collaboration], *Search for a Standard Model Higgs boson in the mass range 200–600 GeV in the $H \to ZZ \to \ell^+\ell^- q\bar{q}$ decay channel with the ATLAS detector*, Phys. Lett. B **717** (2012) 70 [arXiv:1206.2443 [hep-ex]].

[8] G. Aad *et al.* [ATLAS Collaboration], *Search for the Higgs boson in the $H \to WW \to \ell\nu jj$ decay channel at $\sqrt{s} = 7$ TeV with the ATLAS detector*, Phys. Lett. B **718** (2012) 391 [arXiv:1206.6074 [hep-ex]].

[9] CMS Collaboration, *Search for a Standard Model-like Higgs boson decaying into $WW \to \ell\nu q\bar{q}$ in pp collisions at $\sqrt{s} = 8$ TeV*, CMS-PAS-HIG-13-008.

[10] S. Diglio, *Search for a high-mass Higgs boson using the ATLAS detector*, EPJ Web Conf. **71** (2014) 00038.

[11] V. Khachatryan *et al.* [CMS Collaboration], *Search for a Higgs boson in the mass range from 145 to 1000 GeV decaying to a pair of W or Z bosons*, arXiv:1504.00936 [hep-ex].

[12] M. Pelliccioni [CMS Collaboration], *CMS high-mass WW and ZZ Higgs search with the complete LHC Run 1 statistics*, arXiv:1505.03831 [hep-ex].

[13] E. W. N. Glover and J. J. van der Bij, *Vector boson pair production via gluon fusion*, Phys. Lett. B **219** (1989) 488.

[14] E. W. N. Glover and J. J. van der Bij, *Z-boson pair production via gluon fusion*, Nucl. Phys. B **321** (1989) 561.

[15] T. Binoth, M. Ciccolini, N. Kauer and M. Kramer, *Gluon-induced W-boson pair production at the LHC*, JHEP **0612** (2006) 046 [hep-ph/0611170].

[16] J. M. Campbell, R. K. Ellis and C. Williams, *Gluon-gluon contributions to W^+W^- production and Higgs interference effects*, JHEP **1110** (2011) 005 [arXiv:1107.5569 [hep-ph]].

[17] N. Kauer, *Signal-background interference in $gg \to H \to VV$*, PoS RADCOR **2011** (2011) 027 [arXiv:1201.1667 [hep-ph]].

[18] G. Passarino, *Higgs interference effects in $gg \to ZZ$ and their uncertainty*, JHEP **1208** (2012) 146 [arXiv:1206.3824 [hep-ph]].

[19] N. Kauer and G. Passarino, *Inadequacy of zero-width approximation for a light Higgs boson signal*, JHEP **1208** (2012) 116 [arXiv:1206.4803 [hep-ph]].

[20] M. Bonvini, F. Caola, S. Forte, K. Melnikov and G. Ridolfi, *Signal-background interference effects for $gg \to H \to W^+W^-$ beyond leading order*, Phys. Rev. D **88** (2013) 3, 034032 [arXiv:1304.3053 [hep-ph]].

[21] N. Kauer, *Interference effects for $H \to WW/ZZ \to \ell\bar{\nu}_\ell\bar{\ell}\nu_\ell$ searches in gluon fusion at the LHC*, JHEP **1312** (2013) 082 [arXiv:1310.7011 [hep-ph]].

[22] J. M. Campbell, R. K. Ellis and C. Williams, *Bounding the Higgs width at the LHC using full analytic results for $gg \to e^-e^+\mu^-\mu^+$*, JHEP **1404** (2014) 060 [arXiv:1311.3589 [hep-ph]].

[23] I. Moult and I. W. Stewart, *Jet vetoes interfering with $H \to WW$*, JHEP **1409** (2014) 129 [arXiv:1405.5534 [hep-ph]].

[24] J. M. Campbell, R. K. Ellis and C. Williams, *Bounding the Higgs width at the LHC*, PoS LL **2014** (2014) 008 [arXiv:1408.1723 [hep-ph]].

[25] F. Campanario, Q. Li, M. Rauch and M. Spira, *ZZ+jet production via gluon fusion at the LHC*, JHEP **1306** (2013) 069 [arXiv:1211.5429 [hep-ph]].

[26] J. M. Campbell, R. K. Ellis, E. Furlan and R. Rontsch, *Interference effects for Higgs boson mediated Z-pair plus jet production*, Phys. Rev. D **90** (2014) 9, 093008 [arXiv:1409.1897 [hep-ph]].

[27] C. S. Li, H. T. Li, D. Y. Shao and J. Wang, *Soft gluon resummation in the signal-background interference process of $gg (\to h^*) \to ZZ$*, arXiv:1504.02388 [hep-ph].

[28] F. Cascioli, T. Gehrmann, M. Grazzini, S. Kallweit, P. Maierhofer, A. von Manteuffel, S. Pozzorini, D. Rathlev *et al.*, *ZZ production at hadron colliders in NNLO QCD*, Phys. Lett. B **735** (2014) 311 [arXiv:1405.2219 [hep-ph]].

[29] T. Gehrmann, M. Grazzini, S. Kallweit, P. Maierhofer, A. von Manteuffel, S. Pozzorini, D. Rathlev and L. Tancredi, *W^+W^- production at hadron colliders in next-to-next-to-leading order QCD*, Phys. Rev. Lett. **113** (2014) 21, 212001 [arXiv:1408.5243 [hep-ph]].

[30] S. Liebler, G. Moortgat-Pick and G. Weiglein, *Off-shell effects in Higgs processes at a linear collider and implications for the LHC*, arXiv:1502.07970 [hep-ph].

[31] F. Cascioli, S. Hoche, F. Krauss, P. Maierhofer, S. Pozzorini and F. Siegert, *Precise Higgs-background predictions: merging NLO QCD and squared quark-loop corrections to four-lepton + 0,1 jet production*, JHEP **1401** (2014) 046 [arXiv:1309.0500 [hep-ph]].

[32] G. M. Pruna and T. Robens, *The Higgs Singlet Extension parameter space in the light of the LHC discovery*, Phys. Rev. D **88** (2013) 115012 [arXiv:1303.1150 [hep-ph]].

[33] T. Robens and T. Stefaniak, *Status of the Higgs Singlet Extension of the Standard Model after LHC Run 1*, Eur. Phys. J. C **75** (2015) 3, 104 [arXiv:1501.02234 [hep-ph]].

[34] A. Falkowski, C. Gross and O. Lebedev, *A second Higgs from the Higgs portal*, JHEP **1505** (2015) 057 [arXiv:1502.01361 [hep-ph]].

[35] D. Lopez-Val and T. Robens, Δr and the W-boson mass in the Singlet Extension of the Standard Model, Phys. Rev. D **90** (2014) 11, 114018 [arXiv:1406.1043 [hep-ph]].

[36] V. Martin-Lozano, J. M. Moreno and C. B. Park, *Resonant Higgs boson pair production in the $hh \to b\bar{b}\,WW \to b\bar{b}\ell^+\nu\ell^-\bar{\nu}$ decay channel*, arXiv:1501.03799 [hep-ph].

[37] C. Englert, Y. Soreq and M. Spannowsky, *Off-shell Higgs coupling measurements in BSM scenarios*, JHEP **1505** (2015) 145 [arXiv:1410.5440 [hep-ph]].

[38] E. Maina, *Interference effects in heavy Higgs production via gluon fusion in the Singlet Extension of the Standard Model*, JHEP **1506** (2015) 004 [arXiv:1501.02139 [hep-ph]].

[39] A. Ballestrero and E. Maina, *Interference effects in Higgs production through vector boson fusion in the Standard Model and its Singlet Extension*, arXiv:1506.02257 [hep-ph].

[40] C. Englert, I. Low and M. Spannowsky, *On-shell interference effects in Higgs boson final states*, Phys. Rev. D **91** (2015) 7, 074029 [arXiv:1502.04678 [hep-ph]].

[41] http://gg2VV.hepforge.org/

[42] T. Binoth and J. J. van der Bij, *Influence of strongly coupled, hidden scalars on Higgs signals*, Z. Phys. C **75** (1997) 17 [hep-ph/9608245].

[43] R. Schabinger and J. D. Wells, *A minimal spontaneously broken hidden sector and its impact on Higgs boson physics at the Large Hadron Collider*, Phys. Rev. D **72** (2005) 093007 [hep-ph/0509209].

[44] B. Patt and F. Wilczek, *Higgs-field portal into hidden sectors*, hep-ph/0605188.

[45] M. Bowen, Y. Cui and J. D. Wells, *Narrow trans-TeV Higgs bosons and $H \to hh$ decays: Two LHC search paths for a hidden sector Higgs boson*, JHEP **0703** (2007) 036 [hep-ph/0701035].

[46] V. Barger, P. Langacker, M. McCaskey, M. J. Ramsey-Musolf and G. Shaughnessy, *LHC phenomenology of an extended Standard Model with a real scalar singlet*, Phys. Rev. D **77** (2008) 035005 [arXiv:0706.4311 [hep-ph]].

[47] V. Barger, P. Langacker, M. McCaskey, M. Ramsey-Musolf and G. Shaughnessy, *Complex Singlet Extension of the Standard Model*, Phys. Rev. D **79** (2009) 015018 [arXiv:0811.0393 [hep-ph]].

[48] G. Bhattacharyya, G. C. Branco and S. Nandi, *Universal doublet-singlet Higgs couplings and phenomenology at the CERN Large Hadron Collider*, Phys. Rev. D **77** (2008) 117701 [arXiv:0712.2693 [hep-ph]].

[49] S. Dawson and W. Yan, *Hiding the Higgs boson with multiple scalars*, Phys. Rev. D **79** (2009) 095002 [arXiv:0904.2005 [hep-ph]].

[50] S. Bock, R. Lafaye, T. Plehn, M. Rauch, D. Zerwas and P. M. Zerwas, *Measuring hidden Higgs and strongly-interacting Higgs scenarios*, Phys. Lett. B **694** (2010) 44 [arXiv:1007.2645 [hep-ph]].

[51] P. J. Fox, D. Tucker-Smith and N. Weiner, *Higgs friends and counterfeits at hadron colliders*, JHEP **1106** (2011) 127 [arXiv:1104.5450 [hep-ph]].

[52] C. Englert, T. Plehn, D. Zerwas and P. M. Zerwas, *Exploring the Higgs portal*, Phys. Lett. B **703** (2011) 298 [arXiv:1106.3097 [hep-ph]].

[53] C. Englert, J. Jaeckel, E. Re and M. Spannowsky, *Evasive Higgs maneuvers at the LHC*, Phys. Rev. D **85** (2012) 035008 [arXiv:1111.1719 [hep-ph]].

[54] B. Batell, S. Gori and L. T. Wang, *Exploring the Higgs portal with 10/fb at the LHC*, JHEP **1206** (2012) 172 [arXiv:1112.5180 [hep-ph]].

[55] C. Englert, T. Plehn, M. Rauch, D. Zerwas and P. M. Zerwas, *LHC: standard Higgs and hidden Higgs*, Phys. Lett. B **707** (2012) 512 [arXiv:1112.3007 [hep-ph]].

[56] R. S. Gupta and J. D. Wells, *Higgs boson search significance deformations due to mixed-in scalars*, Phys. Lett. B **710** (2012) 154 [arXiv:1110.0824 [hep-ph]].

[57] M. J. Dolan, C. Englert and M. Spannowsky, *New Physics in LHC Higgs boson pair production*, Phys. Rev. D **87** (2013) 5, 055002 [arXiv:1210.8166 [hep-ph]].

[58] B. Batell, D. McKeen and M. Pospelov, *Singlet neighbors of the Higgs boson*, JHEP **1210** (2012) 104 [arXiv:1207.6252 [hep-ph]].

[59] J. M. No and M. Ramsey-Musolf, *Probing the Higgs portal at the LHC through resonant di-Higgs production*, Phys. Rev. D **89** (2014) 9, 095031 [arXiv:1310.6035 [hep-ph]].

[60] S. Profumo, M. J. Ramsey-Musolf, C. L. Wainwright and P. Winslow, *Singlet-catalyzed electroweak phase transitions and precision Higgs boson studies*, Phys. Rev. D **91** (2015) 3, 035018 [arXiv:1407.5342 [hep-ph]].

[61] H. E. Logan, *Hiding a Higgs width enhancement from off-shell gg $(\to h^*) \to ZZ$ measurements*, arXiv:1412.7577 [hep-ph].

[62] C. Y. Chen, S. Dawson and I. M. Lewis, *Exploring resonant di-Higgs boson production in the Higgs Singlet Model*, Phys. Rev. D **91** (2015) 3, 035015 [arXiv:1410.5488 [hep-ph]].

[63] S. Heinemeyer *et al.* [LHC Higgs Cross Section Working Group Collaboration], *Handbook of LHC Higgs Cross Sections: 3. Higgs Properties*, arXiv:1307.1347 [hep-ph].

[64] CMS Collaboration, *Search for the resonant production of two Higgs bosons in the final state with two photons and two bottom quarks*, CMS-PAS-HIG-13-032.

[65] CMS Collaboration, *Search for di-Higgs resonances decaying to 4 bottom quarks*, CMS-PAS-HIG-14-013.

[66] T. Hahn, *Generating Feynman diagrams and amplitudes with FeynArts 3*, Comput. Phys. Commun. **140** (2001) 418 [arXiv:hep-ph/0012260].

[67] T. Hahn and M. Perez-Victoria, *Automatized one-loop calculations in four and D dimensions*, Comput. Phys. Commun. **118** (1999) 153 [arXiv:hep-ph/9807565].

[68] C. Degrande, C. Duhr, B. Fuks, D. Grellscheid, O. Mattelaer and T. Reiter, *UFO - The universal FeynRules output*, Comput. Phys. Commun. **183** (2012) 1201 [arXiv:1108.2040 [hep-ph]].

[69] A. Alloul, N. D. Christensen, C. Degrande, C. Duhr and B. Fuks, *FeynRules 2.0 - A complete toolbox for tree-level phenomenology*, Comput. Phys. Commun. **185** (2014) 2250 [arXiv:1310.1921 [hep-ph]].

[70] A. D. Martin, W. J. Stirling, R. S. Thorne and G. Watt, *Parton distributions for the LHC*, Eur. Phys. J. C **63** (2009) 189 [arXiv:0901.0002 [hep-ph]].

[71] S. Dittmaier *et al.*, *Handbook of LHC Higgs cross sections: 1. Inclusive observables*, arXiv:1101.0593 [hep-ph].

[72] S. Goria, G. Passarino and D. Rosco, *The Higgs boson lineshape*, Nucl. Phys. B **864** (2012) 530 [arXiv:1112.5517 [hep-ph]].

[73] F. A. Berends, R. Pittau and R. Kleiss, *All electroweak four fermion processes in electron - positron collisions*, Nucl. Phys. B **424** (1994) 308 [hep-ph/9404313].

[74] N. Kauer, C. O'Brien and E. Vryonidou, *Interference effects for $H \to WW \to \ell\nu q\bar{q}'$ and $H \to ZZ \to \ell\bar{\ell}q\bar{q}$ searches in gluon fusion at the LHC*, arXiv:1506.01694 [hep-ph].